Nanopatterning by multiple-ion-beam sputtering

2009 J. Phys.: Condens. Matter 21 224011

(http://iopscience.iop.org/0953-8984/21/22/224011)

IOP Publishing Journal of Physics: Condensed Matter

J. Phys.: Condens. Matter **21** (2009) 224011 (8pp) doi:10.1088/0953-8984/21/22/224011

TOPICAL REVIEW

Nanopatterning by multiple-ion-beam sputtering

M Joe[1], J-H Kim[2], C Choi[1], B Kahng[1] and J-S Kim[2]

[1] Department of Physics and Astronomy, Seoul National University, Seoul 151-747, Korea
[2] Department of Physics, Sook-Myung Women's University, Seoul 140-742, Korea

E-mail: jskim@sookmyung.ac.kr

Received 28 January 2009
Published 12 May 2009
Online at stacks.iop.org/JPhysCM/21/224011

Abstract

We conducted a systematic study on nanopatterning by multiple-ion-beam sputtering, focusing on the superposition of the simple patterns formed by individual ion beams. When Au(001) is simultaneously sputtered by two ion beams at grazing incidence, both nanodot and nanohole patterns are obtained. If a rippled surface is subsequently sputtered at normal incidence, a nanobead pattern is obtained. All of the obtained patterns consist of the nanopatterns formed by individual ion beams; however, the superposition of nanopatterns is not realized in its ideal form. We also discuss the microscopic mechanism of pattern formation by multiple-ion-beam sputtering, and consider the questions and possibilities remaining to be explored.

(Some figures in this article are in colour only in the electronic version)

Contents

1. Introduction

Ion-beam sputtering (IBS), widely applied in the fabrication of self-organized nanostructures, can be applied to almost all materials, including insulators, metals, and even organic materials, and is manipulated by easily controllable physical parameters [1]. This physical self-assembly is distinct from the self-organized growth of organic and bio-materials, which is only applicable to limited classes of materials and is controlled by chemical and thermodynamic variables.

The patterns currently able to be formed by IBS are limited to symmetric hexagonal or square patterns of dots, holes, or ripples. If the incident ion beam is oriented nearly normal to the surface, two-dimensional (2D) patterns of nanodots [2–6] or nanoholes [7, 8] are formed. By oblique incidence of the ion beam, periodic ripples can be produced on the irradiated surface [9–22]. It appears that only the most basic structures can be produced by IBS; therefore, novel approaches are urgently required to obtain the more complex and structurally versatile patterns needed for the tailored nano-sculpting of surfaces.

To date, sputter-induced patterning has been performed using a single ion beam under fixed sputter geometry, although in one case a rotating substrate was used [23]. This practice employed in IBS may represent one of the factors that limits the diversity of IBS-induced patterns. To increase the range of achievable nanopatterns, Carter [24] proposed the use of dual-ion-beam sputtering (DIBS) to induce interference patterns, although this idea has yet to be fully tested experimentally.

Recently, Vogel and Linz investigated the possibility of nanopatterning by multiple-ion-beam sputtering [25]. The authors started from the damped Kuramoto–Sivashinsky (dKS) equation and predicted the formation of various surface patterns by adjusting the parameters that determine the strength of the damping γ and ion-induced effective surface diffusion δ. The parameters γ and δ can be controlled in experiments by, for example, tuning the incident angles of

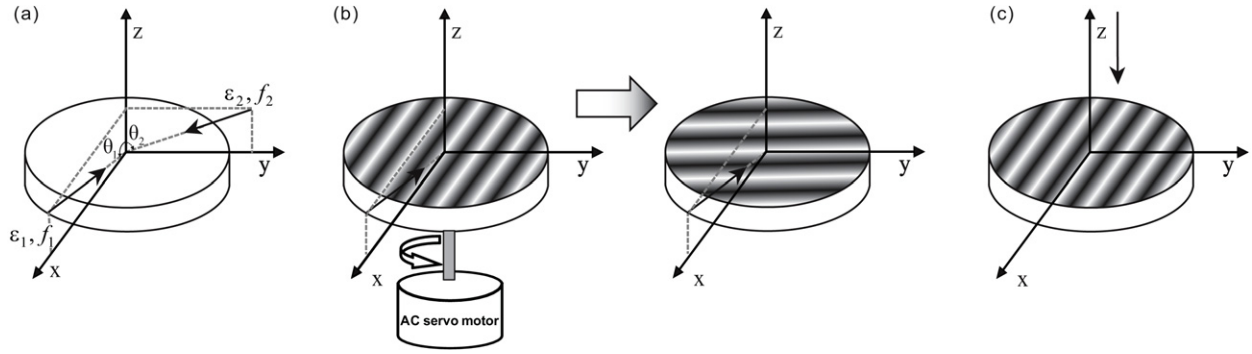

Figure 1. Schematic illustration of the three different modes of multiple-ion-beam sputtering considered in this study.

the four ion beams. As an alternative, the authors also suggest the possibility of the sequential application of an ion beam, with the sample held in different orientations with respect to the beam at each application, in order to fabricate sophisticated nanopatterns [25]. To date, however, few experimental studies have considered patterning by multiple-ion-beam sputtering [26–28].

In this report, we present the experimental results of multiple-ion-beam sputtering of Au(001) performed in three different ways: a case of DIBS and two cases of sequential ion-beam sputtering (SIBS). In the DIBS approach, two ion beams were simultaneously incident on Au(001) at a grazing angle and oriented perpendicular to each other in azimuth (figure 1(a)). In the SIBS approach, we sputtered the sample in a single direction using a single ion beam (at the same grazing angle as that used for DIBS) to form ripples on the substrate. The rippled surface was then rotated by 90° in azimuth while maintaining the polar angle, and sputtered again (figure 1(b)). In the second SIBS experiment, the rippled surface was further sputtered by an ion beam oriented normal to the surface (figure 1(c)).

The DIBS experiment yielded 2D patterns of nanoholes and nanodots (without ripples), although it must be remembered that sputtering was made at a grazing angle with the sample at rest [26]. In the diffusive regime, where energy and flux are relatively weak and pattern formation is largely governed by diffusion of the main surface species, a square-symmetric pattern of nanoholes is formed, where the edges of the squares are aligned along the directions of high symmetry in the substrate. In the erosive regime, beam energy and beam flux are sufficiently large that erosion is the dominant effect in the patterning process. In this case, pattern orientation is independent of the crystallographic directions of the substrate; instead, it relates to the direction of the ion beam.

For the case of SIBS with crossing ion-beam sputtering (CIBS) of the pre-rippled surface [27] (figure 1(b)), we observed a rapid decay of the initial ripple and the growth of new ripples in the direction of the crossing ion beam. No interference pattern of crossing ripples was observed under either the erosive or diffusive regimes. For the other case of SIBS, involving IBS oriented normal to the pre-rippled surface [28] (figure 1(c)), we observed a pattern of nanodots arranged along the underlying ripples or nanobeads. This nanobead pattern appears to result from the superposition of ripples and dots that formed consecutively by sputtering at a grazing angle and by subsequent normal-incidence sputtering, respectively. However, the wavelength of the ripple in the nanobead pattern is larger than that of the initial ripple, and the dots form only on the crests of the ripples. This nanobead pattern is a salient feature, raising the possibility that SIBS will enable new schemes to fabricate sophisticated nanopatterns.

We also studied the mechanism of pattern formation by multiple-ion-beam sputtering, following the approach of Bradley and Harper [29]. In their model, the diffusion of adatoms and vacancies is considered according to the theory of Mullins [30] and sputter erosion is considered according to the theory of Sigmund [31].

We applied the BH approach to the DIBS method, and derived a continuum equation with the same form as the Kuramoto–Sivashinsky (KS) equation for the present DIBS geometry, although with different coefficients. The most notable feature of the KS equation for DIBS is that it does not induce growth instability, in contrast to the observed patterns generated by DIBS. For the SIBS case, a numerical analysis using the KS equation does not reproduce the observed pattern evolution. The results of these two theoretical studies suggest that pictures beyond that of BH are needed to describe the processes involved in pattern formation by multiple-ion-beam sputtering. We also discuss ways to overcome the limitations of the BH-type approach.

2. Experiment

All sputtering experiments were performed in a custom-built ultrahigh-vacuum chamber. The base pressure of the chamber is in the range of mid to high 10^{-10} Torr. Clean and atomically flat Au(001) surfaces were prepared by a series of Ar^+ sputtering and annealing cycles with an annealing temperature of 730 K. The mean terrace width of the clean Au(001) was in the order of several hundred nanometers.

During both DIBS and the grazing-angle sputtering in SIBS, the impinging ion beams make a grazing angle to the surface normal of $\theta \approx 73°$ (figure 1). Each ion gun is mounted on a goniometer that enables adjustment of the incident angle in two perpendicular directions. The ion energy ϵ and ion flux f for each ion beam are operated in two modes: (i) $\epsilon = 0.5$ keV and relatively small flux

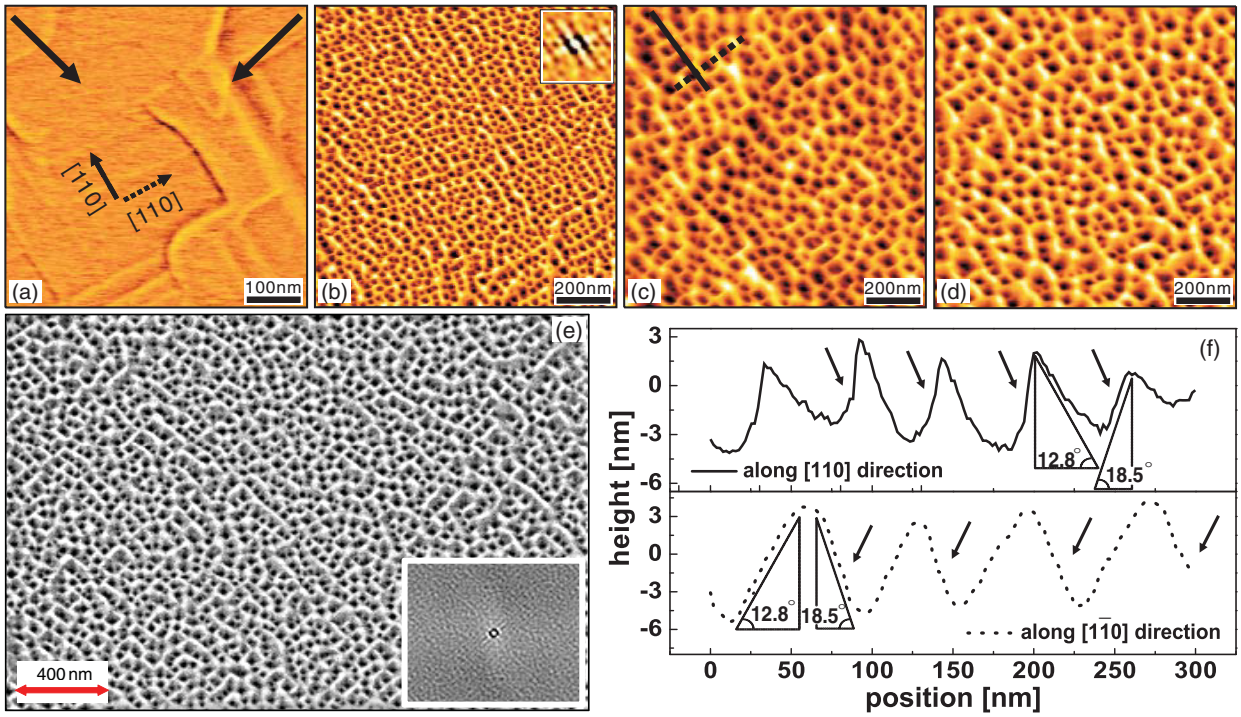

Figure 2. (a) Initial Au(001) sample. (b)–(d) Nanopatterns induced by DIBS under the diffusive regime, $\epsilon = 0.5$ keV and $f = f_1 + f_2 = 0.93$ ions nm^{-2} s^{-1}. The figures are presented in order of increasing fluence. (b) $\Psi = 5.2 \times 10^3$ nm^{-2}, (c) $\Psi = 2.0 \times 10^4$ nm^{-2}, (d) $\Psi = 3.5 \times 10^4$ nm^{-2}. (e) Representative SEM image taken at $\Psi = 2.0 \times 10^4$ nm^{-2} and corresponding autocorrelation function (inset). (f) Height profiles along the two lines marked in (c). Arrows indicate the incident ion-beam directions.

($f < 1$ ion nm^{-2} s^{-1} for DIBS and $f < 0.1$ ion nm^{-2} s^{-1} for CIBS), and (ii) $\epsilon = 2.0$ keV and relatively large flux ($f > 1$ ion nm^{-2} s^{-1} for DIBS and $f > 0.1$ ion nm^{-2} s^{-1} for CIBS)[3]. The former case corresponds to the diffusive regime and the latter to the erosive regime [32]. A minor increase in sample temperature (less than 20 K) from the initial temperature (room temperature) was observed at the last stage of sputtering because of thermal accumulation associated with extended sputtering. The morphological evolution of Au(001) by IBS was investigated *ex situ* by atomic force microscopy in contact mode.

3. Dual-ion-beam sputtering

DIBS in the diffusive regime. Figure 2 shows the development of nanopatterns on Au(001) by DIBS in the order of increasing ion fluence Ψ ($=f \times t$). Figure 2(a) shows a representative initial Au(001) displaying wide terraces with an average width of several hundred nanometers. For $\Psi \approx 5.2 \times 10^3$ nm^{-2}, ordered holes are clearly visible in figure 2(b). The holes are closely packed and have four-fold symmetry, with edges along the {110} directions (see inset in figure 2(b)). The inset shows the height–height correlation function $G(\mathbf{d}) = \langle h(\mathbf{r})h(\mathbf{r}+\mathbf{d})\rangle$, where $\langle\cdot\rangle$ denotes the spatial average and $\mathbf{d}$ is displacement. Each hole is enclosed by four sub-linear ridges, suggesting that the pattern originates from crossing ripples; however, the ridges are aligned along the densely packed {110} crystallographic direction rather than along the beam directions (marked by arrows in figure 2(a)). This finding indicates that the nanopatterning is governed by the diffusion of surface species. As the ion fluence increases further (figures 2(c) and (d)), lateral and vertical growth of the holes is observed, and the symmetry and order of the nanopatterns show a gradual decrease, possibly reflecting the accumulation of thermal agitation. Figure 2(e) shows a wider view obtained by scanning electron microscope, confirming the formation of a nanohole pattern. The uniformity and long-range order of the pattern are also more clearly observed in this image.

Such nanohole arrays have been reported previously for various materials [33, 34], although with relatively poor lateral order because nanohole arrays form in the diffusive regime by thermally activated vacancies. The relatively high order of the present nanohole pattern may be attributed to the preferential diffusion of vacancies along ripples that offer highly efficient diffusion channels along their step edges. To improve the order of sputtered patterns, recent studies have explored the sputtering of pre-patterned surfaces [35]. In this context, during DIBS we witnessed self-templating (by the ripples) and the self-organized growth of nanoholes.

Figure 2(f) shows representative line profiles along the two crystallographic directions marked by solid and dashed lines in figure 2(c). Comparison of the two profiles reveals that ridges along [1$\bar{1}$0] (solid line) are broader than those along [110]

[3] The total flux is doubled during DIBS, and thus the temperature rise of the sample is higher than during CIBS. To compensate the enhanced diffusion during DIBS, a larger f is required to reach the erosive condition than that during CIBS. The referred f is a nominal value estimated from the integrated fluxes over the entire irradiated area, which extends further beyond the sample area due to both the grazing incidence and the defocused operation of the ion gun for uniform irradiation of the sample.

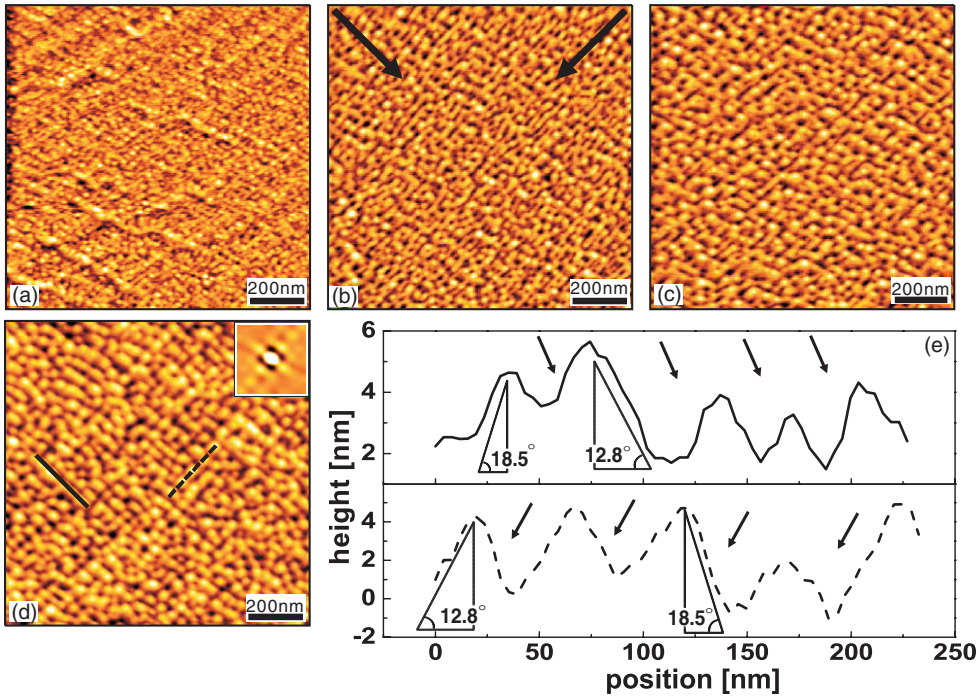

Figure 3. Nanopatterns induced by DIBS under the erosive regime, $\epsilon = 2$ keV and $f \approx 3.25$ ions nm^{-2} s^{-1}. (a)–(d) are presented in order of increasing fluence. (a) $\Psi = 940$ nm^{-2}, (b) $\Psi = 1900$ nm^{-2}, (c) $\Psi = 3900$ nm^{-2}, and (d) $\Psi = 6350$ nm^{-2}. The inset in (d) shows the height–height correlation function. (e) Height profiles along the two lines marked in (d). Arrows indicate the incident ion-beam directions.

(dashed line). The mean wavelengths along $[1\bar{1}0]$ and [110], as estimated from the height–height correlation function, are 65 ± 3 and 54 ± 2 nm, respectively, reflecting the difference between the two ion beams employed for DIBS. Another distinguishable feature is that the ridges show slope selection, with different slopes on opposing faces (figure 2(f)): the (1,1,4) facet is frequently found on the illuminated (by the crossing ion beam) side, while the (1,1,6) facet is found on the shadow side. Similarly asymmetric ripple slopes are also observed for ripples formed in the erosive regime (figure 3(e)). It is tempting to attribute this asymmetry to the slope dependence [36, 37] of the erosion rate as the ion beam crosses the ripple; however, the different erosion rates of the two sides only affect their lateral erosion rates. As long as the erosion rate is uniform on each side, the slopes remain unchanged. This finding indicates the likely existence of effects that are dependent on the incident angle (in addition to sputter erosion) and that produce asymmetric slopes.

DIBS in the erosive regime. Ordered patterns of nanodots develop in the erosive regime (figure 3). Figure 3(a) shows the incipient stage of nanodot formation, revealing tiny dots of various sizes and shapes. In some regions, the dots already show the square-symmetric order of the nanodots. With increasing Ψ, the dots grow and are more easily discernable, but most remain linked to each other (figure 3(b)). In figure 3(c), openings are locally present, and the pattern resembles a labyrinth (figure 3(c)). With further sputtering, a pattern of separated dots emerges (figure 3(d)). The dots are reasonably well ordered and show square-symmetric correlations, as shown in the height–height correlation (inset in figure 3(d); however, the dot size is highly variable and there are many point defects that are largely more/less than four-coordinated.

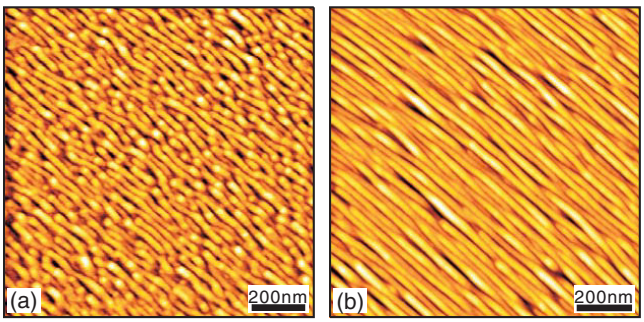

Figure 4. Nanopatterns induced by DIBS with unbalanced dual beams (a) and single IBS (b). For the case of DIBS, the beam fluxes are varied from that for figure 3(d): f_1 is decreased by about 5% and f_2 is increased by about 30%. For (b), the beam flux is the same as f_2 in (a).

It is noteworthy that in the erosive regime the 2D pattern of nanodots (as seen in figure 3) is achieved only under the balance of the two ion beams; otherwise, modulated ripples are observed (see figure 4(a)). The 2D nanohole pattern, on the other hand, is formed in the diffusive regime with no strict requirements for the balance of the two ion beams. The modulated ripples are markedly different from the ripples formed by single-ion-beam sputtering, which show no modulation in height and width (figure 4(b)). The observed modulation in figure 4(a) is suggestive of the incomplete breakage of ripples into dots by the crossing (minor) ion beam of lesser flux.

We explain the distinct behaviors under the two sputtering conditions as follows. The role of each ion beam during DIBS is two-fold: each beam produces ripples along its direction while simultaneously destroying perpendicular ripples. If a balance is not achieved between the two beams, then one beam (the major beam) breaks a crossing ripple into nanodots, while the other (minor) beam is incapable of breaking the crossing ripple into separate nanodots, instead resulting in modulation. As a result, the nanodot pattern is observable only under highly restricted conditions in which both beams break their crossing ripples into nanodots simultaneously. In the diffusive regime, however, diffusion of the adatoms and/or vacancies along the edges of the ripples occurs so rapidly [32] that the ripple defects caused by the crossing ion beam are efficiently cured. Thus, the ripples in both directions are able to maintain their shape, forming ripple-bound holes under most sputtering conditions. In short, the instability that forms a nanodot array from a ripple is absent in the diffusive regime.

Does the superposition of crossing ripples occur during DIBS? It would be interesting to determine whether the pattern induced by DIBS results from the superposition of the two crossing ripples, each of which is independently formed by the respective ion beam employed for DIBS [24, 25]. To address this issue, we performed ripple formation independently for each ion beam employed for DIBS (under the same DIBS conditions) and digitally superposed the two ripple patterns. We then compared the new image with the DIBS image.

Figure 5(a) shows the pattern obtained by DIBS under diffusive conditions, while figure 5(b) shows the digitally superposed image consisting of two independently formed ripple patterns. We also obtained a DIBS pattern (figure 5(c)) and superposed image (figure 5(d)) under the erosive regime. For both regimes, the superposed images do not resemble the DIBS images, which show larger characteristic lengths and spacings. Moreover, in the diffusive regime the nano-features in the real image are nanoholes rather than the nanodots observed in the superposed image, and the instability of the nanodot pattern observed under the erosive regime is not apparent in the superposed pattern. Taken together, the above observations indicate that superimposing the ripples that form during DIBS is an invalid approach.

One might wonder, however, whether the increase in the characteristic length in both regimes reflects an increase in substrate temperature arising from the doubled flux in DIBS compared with that in single ion-beam sputtering. In fact, we observe an increase in sample temperature of $\leqslant$20 K at the end of each sputtering term relative to the original temperature. According to the linear theory proposed by Bradley and Harper [29], the ripple wavelength follows $\ell \propto \sqrt{2\,\mathrm{K}\exp(-E/k_\mathrm{B}T)}$, where K is the thermal diffusion constant, E the relevant diffusion barrier, k_B the Boltzmann constant, and T the substrate temperature. Indeed, by using the known terrace diffusion barrier on Au(001), whereby $E \approx 0.65$ eV [38], we estimate the increase in the characteristic size to be approximately 112%, corresponding to a 20 K increase in substrate temperature. Thus, the enhanced temperature can explain the discrepancy in characteristic length between the DIBS pattern and the superposed ripple pattern.

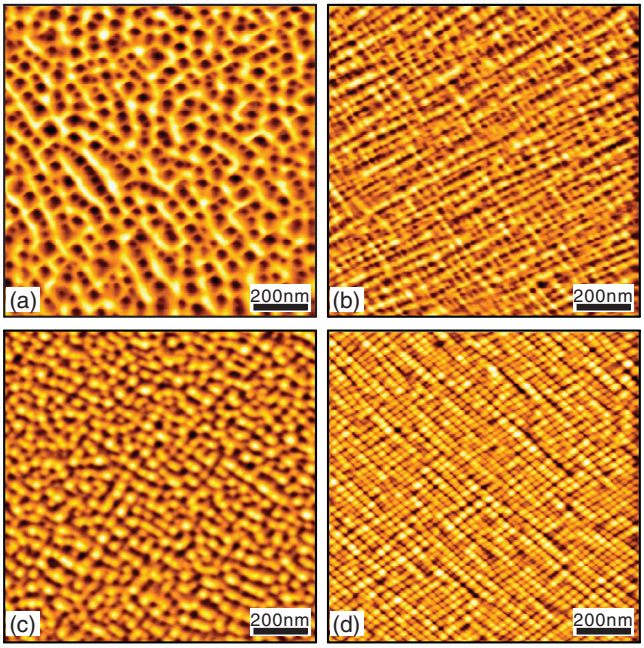

Figure 5. Nanopatterns formed by DIBS under the diffusive (a) and erosive (c) regimes. (a) is obtained from figure 2(d), and (c) from figure 3(d). (b) and (d) are digitally superposed images for the diffusive and erosive regimes, respectively.

Furthermore, with increasing substrate temperature the species shaping surface may change from adatoms to vacancies, as the diffusion barrier for advacancy is higher than that for adatom [7, 39]. In fact, such a change in surface structure from adatom islands to vacancy islands has been reported previously with an increase in substrate temperature [7, 39, 40]. The ion flux is lower for the diffusive regime than for the erosive regime; consequently, the effective temperature that approximately scales inversely to the flux [41] should be higher in the former than in the latter. Accordingly, the switch in surface species is likely to occur (and is actually observed) in the diffusive regime. In short, thermal effects are critical in shaping Au(001) during sputtering, whereas the present experiments were performed without the temperature being fully stabilized. Before reaching a firm conclusion regarding whether the superposition of ripples works during DIBS, further experiments are required in which substrate temperature is carefully controlled.

Microscopic picture of DIBS. To obtain a microscopic picture of DIBS, we established a continuum equation following the scheme of Bradley and Harper. We apply the Sigmund theory for sputtering to the case in which two ion beams are incident simultaneously: the normal erosion velocity V_o at a generic point o on the surface is described simply by superposition of the two energy dissipation functions corresponding to the two ion beams: $V_o \propto \int \mathrm{d}\mathbf{r}\,\{\varepsilon_1(\mathbf{r})\,f_1(\mathbf{r}) + \varepsilon_2(\mathbf{r})\,f_2(\mathbf{r})\}$, where dissipation of the impact energy $\varepsilon(\mathbf{r})$ is represented by the Gaussian function with widths of σ along the incident ion direction and μ in the lateral plane perpendicular to this direction [31, 42]. This calculation does not take into account any correlation effect between the two beams.

Table 1. Coefficients of the KS equation, estimated by the TRIM algorithm under the experimental conditions. All values are per unit flux.

	ν_x (Å)	ν_y (Å)	D_{xx} (Å^3)	D_{yy} (Å^3)	D_{xy} (Å^3)
SIBS in x	14.2	−0.9	−2888.4	38.5	−939.1
SIBS in y	−0.9	14.2	38.5	−2888.4	−939.1
DIBS with $r = 1$	13.3	13.3	−2849.9	−2849.9	−1878.2

The resulting continuum equation remains in the same form as the KS equation provided that the azimuthal angle between the two incident beams is 90°, although the coefficient of each term is modified to reflect DIBS. In the general case of DIBS, detailed formulae are given in [43]. The KS equation reads as follows:

$$\frac{\partial h}{\partial t} = \nu_x \nabla_x^2 h + \nu_y \nabla_y^2 h - D_{xx} \nabla_x^4 h - D_{xy} \nabla_x^2 \nabla_y^2 h - D_{yy} \nabla_y^4 h - K \nabla^4 h + \lambda_x (\nabla_x h)^2 + \lambda_y (\nabla_y h)^2 + \eta(x, y, t). \quad (1)$$

Here, ν is the effective surface tension generated by the erosion process and D is the ion-induced effective diffusion constant [41]. λ is the tilt-dependent erosion rate [44] and η is uncorrelated white noise with a zero mean, mimicking the randomness resulting from the stochastic nature of ion arrival at the surface [45]. For the KS equation for DIBS, the coefficients ν and D are determined as follows; $\nu_x^{(\mathrm{DIBS})} = \nu_x^{(x)} + r\nu_x^{(y)}$, where $\nu_i^{(x)}$ is the coefficient of the $\nabla_i^2 h$ term when a single ion beam is incident along the x direction, and $r = f_2/f_1$. $\nu_y^{(\mathrm{DIBS})}$ and $D^{(\mathrm{DIBS})}$ are determined in a similar manner.

The numerical value of each coefficient is estimated by TRIM analysis [46] under the experimental condition [26], and the results are summarized in table 1. Because D_{xx} and D_{yy} are very large in absolute magnitude due to sputter-induced diffusion, the coefficients $\nabla^2 h$, $\nu_x^{(\mathrm{DIBS})}$, and $\nu_y^{(\mathrm{DIBS})}$ become positive, and $D_{xx}^{(\mathrm{DIBS})}$ and $D_{yy}^{(\mathrm{DIBS})}$ are negative. Thus, the linear instability condition for the KS equation no longer holds for DIBS, in contrast to experimental observations. Hence, the KS equation for DIBS fails to explain pattern formation by DIBS.

The discrepancy between the stable surface predicted by the KS equation for DIBS and the observed nanopattern may be resolved within the KS picture if a cross term exists in the form of $\partial_x \partial_y h$, as this can yield a different dispersion relation in the linear instability analysis. In fact, the cross term was proposed in [25] to take into account the interference effect between the two beams, even though this effect was considered in the damped KS equation. In our case, we described DIBS by adding the Sigmund energy dissipation functions of the two beams; we neglected higher-order correlations of the sputter events. It is necessary to carefully examine the types of correlation effects that are possible, as well as how they can be represented in continuum theory. The cross term can also be obtained in the KS equation for DIBS if the azimuthal angle between the two ion beams deviates from 90°. It is possible that there exists dispersion in the direction of each ion beam in the experiment, and therefore that the angle between them would vary by about 90°. In such a case, the cross term might remain effective, and instability in surface growth might still hold in DIBS, thereby yielding the pattern observed in the present experiment.

From a theoretical perspective, we remain cautious about oversimplifying the treatment of sputtering events during DIBS. Each ion beam during DIBS hits the crossing ripples with a large difference in incidence angle between the illuminated and shadow sides. In terms of the morphological evolution of such a highly modulated surface, it is essential to use a nonlinear term that takes into account the dependence of erosion rate V_o on the local slope [47]. This suggests that the linear instability argument may not be applicable in the present experimental situation. Finally, redeposition of the sputtered atoms is not included in the KS equation for DIBS; however, the results of recent experiments [6], hydrodynamic modeling [37], and molecular dynamic simulations [48] indicate their significant contribution to the morphological evolution of the surface during ion-beam sputtering.

4. Sequential ion-beam sputtering

The simultaneous incidence of multiple ion beams on a surface is limited in its variety by the port arrangement of the sample-preparation chamber. Moreover, it is difficult to obtain precise control of each ion beam to dose the required flux with a well-defined incidence angle, although such control is sometimes demanded, as indicated by the high sensitivity of DIBS patterns to the balance of the two ion beams (figure 4). An alternative approach involves the sequential application of a single ion beam to a sample surface whose orientation with respect to the ion beam is varied in a controlled manner [25]. In a numerical study of the damped Kuramoto–Sivashinsky equation, Vogel and Linz [25] predicted that various nanopatterns could be obtained by SIBS. The orientation of a sample can be precisely and reproducibly controlled during an experiment, meaning that SIBS can be performed in a well-defined manner.

SIBS can be realized by various combinations of sample orientations relative to the ion beam. As a very simple case, we first sputtered a sample in the close packed [110] direction of Au(001) with the polar angle fixed at 72° from the normal to the sample surface (figure 2(b)), and formed a ripple pattern. For the next sputtering, we rotated the sample by 90° in azimuth while maintaining the polar angle. Figure 6(a) shows the ripple pattern formed by the initial IBS along the [110] direction of Au(001) under the sputter condition of the erosive regime, similar to that for DIBS. With subsequent sputtering by the crossing ion beam, the initial ripple pattern is heavily damaged such that its order and mean coherence length are severely degraded (figure 6(b)). On the modified ripple pattern, we observe the growth of new ripples along the direction of the crossing ion beam that will prevail upon the surface with

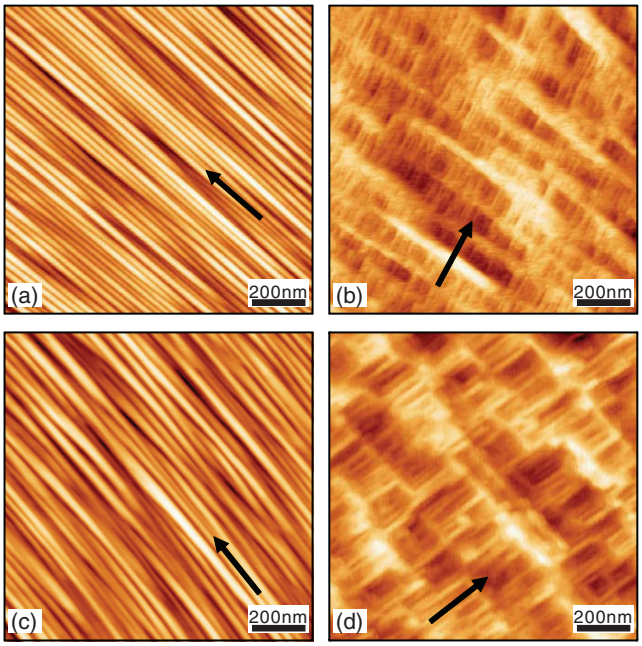

Figure 6. (a) Rippled Au(001) surface in the erosive regime. (b) Surface morphology (induced by CIBS) of the rippled Au(001) in the erosive regime. Sputter conditions were as follows: $\epsilon = 2.0$ keV, $f = 0.31$ ions nm^{-2} s^{-1}, and $\Psi = 84.8$ ions nm^{-2}. (c) Rippled Au(001) surface in the diffusive regime. (d) Surface morphology (induced by CIBS) of the rippled Au(001) in the diffusive regime. Sputter conditions were as follows: $\epsilon = 0.5$ keV, $f = 0.06$ ions nm^{-2} s^{-1}, and $\Psi = 716.3$ ions nm^{-2}. Arrows indicate ion-beam projection.

further IBS. Under the diffusive condition, similar to the case of DIBS, we also observe initial ripple formation (figure 6(c)) and its destruction, followed by new ripple formation along the direction of the crossing ion beam (figure 6(d)). Hence, an immediate conclusion one can make is that the superposition of two ripples formed by IBS in perpendicular directions is not realized under both erosive and diffusive sputtering conditions. This is in contrast to the prediction of a numerical study of the dKS model [25]. The results of molecular dynamic simulations indicate that nonlinear effects such as redeposition play a significant role during pattern evolution in particular if the crossing ion beam is incident on the highly corrugated surface [27, 48]. An accurate description of morphological evolution by SIBS requires adequate treatment of such effects.

As a second example of SIBS, we performed sputtering normal to Au(001) after forming a ripple pattern on the surface. If we achieve a superposition of patterns fabricated by each sputtering, we would expect a ripple pattern overlapped by nanodots or nanoholes. Figure 7(a) shows the ripple pattern formed along [110] under the sputtering condition of the erosive regime, as mentioned above. After sputtering oriented normal to the rippled surface, we obtain a pattern in which nanodots are located on the ripples, which we refer to as nanobeads (figure 7(b)). The nanobead pattern appears to be a realization of the superposition of the nanodot and ripple patterns; however, as the normal-oriented ion-beam sputtering proceeds, the rippled surface becomes smooth and ripples

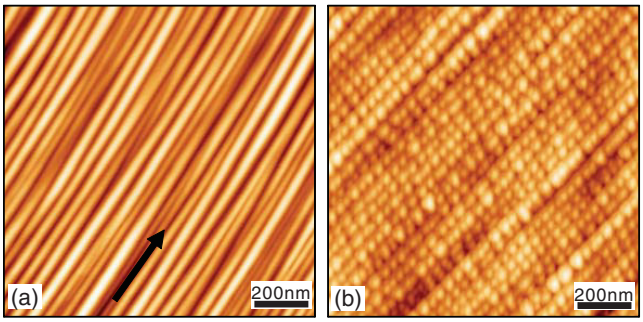

Figure 7. (a) Initial rippled Au(001) pattern and (b) nanobead pattern induced by subsequent IBS oriented normal to the rippled Au(001). The sputter conditions for the initial ripple (nanobead pattern) were as follows: $\epsilon = 2.0$ keV ($\epsilon = 2.0$ keV), $f = 0.31$ ions nm^{-2} s^{-1} ($f = 1.19$ ions nm^{-2} s^{-1}), and $\Psi = 4500$ ions nm^{-2} ($\Psi = 1781$ ions nm^{-2}). The arrow in (a) indicates the projection of the ion beam.

with small (less than 30 nm) widths disappear, resulting in an increase in mean ripple width [28].

From a practical viewpoint, this result is stimulating because two different patterns expected for the two different sputtering geometries are apparently superposed to form a novel pattern (i.e. a nanobead pattern). A second interesting feature is that the nanodot pattern acquires a high degree of one-dimensional order, guided by the ripples as a template. In some regions, the dots on an individual ripple grow in tandem with those on adjacent ripples to form a square-symmetric order of nanodots on ripples. The nanodots formed solely by normal IBS and self-organized themselves into a square-symmetric pattern of much lower order than that of the nanobead obtained by SIBS. This result raises the possibility that a suitable combination of SIBS can produce novel ordered nanopatterns, although an approach involving the superposition of patterns is not applicable in their pristine form.

5. Summary and conclusion

We sputtered Au(001) by dual ion beams and studied the development of the induced pattern. Highly ordered nanopatterns were formed by DIBS: a 2D nanohole array in the diffusive regime and a nanodot array in the erosive regime. In the erosive regime, instability is observed in pattern formation. Careful balancing of the two crossing ion beams is necessary for 2D pattern formation.

We derived a continuum equation from Sigmund theory with two energy dissipation functions to take DIBS into account. For the present DIBS, with two beams that are perpendicular to each other in azimuth, the equation has the same form as the KS equation, although the coefficients are altered to reflect DIBS. The KS equation predicts a stable surface, contrary to experimental observations. We propose several possibilities e.g. redeposition, in terms of improving our understanding of nanopatterning by DIBS.

We also examined the possibility of SIBS for nanopatterning via interference patterns formed in sequence. First, we

formed a ripple pattern along a given direction via the grazing incidence of the ion beam; we then repeated the process at 90° to the initial direction. We did not obtain an interference pattern; instead, the initial pattern was destroyed before new ripples could occur along the ion-beam direction. However, in the case of normal sputtering of a pre-rippled surface, we obtained a pattern of *nanobead*s consisting of nanodots on the existing ripples. This nanobead formation raises the possibility of forming novel nanostructures by SIBS.

Pattern formation by multiple-ion-beam sputtering is not properly explained by conventional theories on sputter-induced patterning based on the Bradley and Harper picture, which combines the sputtering theory of Sigmund and diffusion theory. To accurately describe multiple-ion-beam sputtering and pattern formation, it may be necessary to take into account factors that are currently missing from the BH model, e.g. the correlation effects of ion beams and redeposition.

Acknowledgments

Helpful comments by R Cuerno are gratefully acknowledged. This work was supported by KRF (KRF-2007-314-C00078) and a KOSEF grant funded by MOST (No. R17-2007-073-01001-0).

References

[1] Chan W L and Chason E 2007 *J. Appl. Phys.* **101** 121301
[2] Facsko S, Dekorsy T, Koerdt C, Trappe C, Kurz H, Vogt A and Hartnagel H L 1999 *Science* **285** 1551
[3] Frost F, Ziberi B, Hoche T and Rauschenbach B 2004 *Nucl. Instrum. Methods Phys. Res.* B **216** 9
[4] Mohanta S K and Soni R K 2007 *J. Appl. Phys.* **102** 074313
[5] Lu M, Yang X J, Perry S S and Rabalais J W 2002 *Appl. Phys. Lett.* **80** 2096
[6] Kim T C, Ghim C M, Kim H J, Kim D H, Noh D Y, Kim N D, Chung J W, Yang J S, Chang Y J, Noh T W, Kahng B and Kim J-S 2004 *Phys. Rev. Lett.* **92** 246104
[7] Costantini G, de Mongeot E B, Boragno C and Valbusa U 2001 *Phys. Rev. Lett.* **86** 838
[8] Gago R, Vázquez L, Cuerno R, Varela M, Ballesteros C and Albella J M 2001 *Appl. Phys. Lett.* **78** 3316
[9] Carter G, Nobes M J and Whitton J L 1985 *Appl. Phys.* A **38** 77
[10] Carter G, Vishnyakov V and Nobes M J 1996 *Nucl. Instrum. Methods Phys. Res.* B **115** 440
[11] Rusponi S, Costantini G, Boragno C and Valbusa U 1998 *Phys. Rev. Lett.* **81** 2735
[12] Valbusa U, Boragno C and de Mongeot F B 2002 *J. Phys.: Condens. Matter* **14** 8153
[13] Chan W L, Pavenayotin N and Chason E 2004 *Phys. Rev.* B **69** 245413
[14] Erlebacher J, Aziz M J, Chason E, Sinclair M B and Floro J A 1999 *Phys. Rev. Lett.* **82** 2330
[15] Umbach C C, Headrick R L and Chang K C 2001 *Phys. Rev. Lett.* **87** 246104
[16] Ziberi B, Frost F, Hoche T and Rauschenbach B 2005 *Phys. Rev.* B **72** 235310
[17] Brown A D, Erlebacher J, Chan W L and Chason E 2005 *Phys. Rev. Lett.* **95** 056101
[18] Habenicht S, Bolse W, Lieb K P, Reimann K and Geyer U 1999 *Phys. Rev.* B **60** R2200
[19] Toma A, Buatier de Mongeot F and Valbusa U 2005 *Nucl. Instrum. Methods Phys. Res.* B **230** 551
[20] Wei Q, Lian J, Zhu S, Li W, Sun K and Wang L 2008 *Chem. Phys. Lett.* **452** 124
[21] Flamm D, Frost F and Hirsch D 2001 *Appl. Surf. Sci.* **179** 95
[22] Liu Z X and Alkemade P F A 2001 *Appl. Phys. Lett.* **79** 4334
[23] Frost F, Schindler A and Bigl F 2000 *Phys. Rev. Lett.* **85** 4116
[24] Carter G 2004 *Vacuum* **77** 97
Carter G 2005 *Vacuum* **79** 106
[25] Vogel S and Linz S J 2007 *Phys. Rev.* B **75** 085425
[26] Joe M, Choi C, Kahng B and Kim J-S 2007 *Appl. Phys. Lett.* **91** 233115
[27] Kim J-H, Joe M, Kim S-P, Ha N-B, Kahng B, Lee K-R and Kim J-S, unpublished
[28] Kim J-H, Ha N-B and Kim J-S, unpublished
[29] Bradley R M and Harper J M E 1988 *J. Vac. Sci. Technol.* A **6** 2390
[30] Mullins W W 1957 *J. Appl. Phys.* **28** 333
[31] Sigmund P 1969 *Phys. Rev.* **184** 383
[32] Valbusa U, Boragno C and de Mongeot F B 2003 *Mater. Sci. Eng.* C **23** 201
[33] Ziberi B, Frost F, Rauschenbach B and Hoche T 2005 *Appl. Phys. Lett.* **87** 033113
[34] Frost F, Fechner R, Flamm D, Ziberi B, Frank W and Schindler A 2004 *Appl. Phys.* A **78** 651
[35] Cuenat A, George H B, Chang K C, Blakely J M and Aziz M J 2005 *Adv. Mater.* **17** 2845
[36] Park S, Kahng B, Jeong H and Barabási A L 1999 *Phys. Rev. Lett.* **83** 3486
[37] Muñoz-García J, Castro M and Cuerno R 2006 *Phys. Rev. Lett.* **96** 086101
[38] Yu B D and Scheffler M 1997 *Phys. Rev.* B **56** R15569
[39] Kim T C, Jo M H, Kim Y, Noh D Y, Kahng B and Kim J-S 2006 *Phys. Rev.* B **73** 125425
[40] Malis O, Brock J D, Headrick R L, Yi M-S and Pomeroy J M 2002 *Phys. Rev.* B **66** 035408
[41] Makeev M A and Barabási A-L 1997 *Appl. Phys. Lett.* **71** 2800
[42] Makeev M A, Cuerno R and Barabási A-L 2002 *Nucl. Instrum. Methods Phys. Res.* B **197** 185
[43] Joe M, Choi C, Kahng B, Kwak C Y and Kim J-S 2008 *J. Korean Phys. Soc.* **52** S181
[44] Kardar M, Parisi G and Zhang Y-C 1986 *Phys. Rev. Lett.* **56** 889
[45] Cuerno R and Barabási A-L 1995 *Phys. Rev. Lett.* **74** 4746
[46] Ziegler J F, Biersack J P and Littmark U 1985 *The Stopping and Range of Ions in Solids* (New York: Pergamon) http://www.srim.org
[47] Chen H H, Urquidez O A, Ichim S, Rodriguez L H, Brenner M P and Aziz M J 2005 *Science* **310** 294
[48] Kim S-P, Kim J-S and Lee K-R, unpublished